Carbohydrate Polymers 230 (2020) 115466

Contents lists available at ScienceDirect

Carbohydrate Polymers

journal homepage: www.elsevier.com/locate/carbpol

Exploration of natural polymers for use as green corrosion inhibitors for AZ31 magnesium alloy in saline environment

Saviour A. Umoren*, Moses M. Solomon, A. Madhankumar, Ime B. Obot

Center of Research Excellence in Corrosion, King Fahd University of Petroleum & Minerals, Dhahran, 31261, Saudi Arabia

ARTICLE INFO

Keywords:
Magnesium alloy
Corrosion
Corrosion inhibition
Corrosion inhibitor formulation
Natural polymer
Saline medium

ABSTRACT

Seven natural polymers namely, chitosan (CHI), dextran (Dex), carboxymethyl cellulose (CMC), sodium alginate (ALG), pectin (PEC), hydroxylethyl cellulose (HEC), and Gum Arabic (GA) were screened for anticorrosion property towards AZ31 Mg alloy in 3.5 wt.% NaCl solution. CHI, Dex, CMC, PEC, and GA accelerated the corrosion while ALG and HEC moderately inhibited the corrosion of the alloy. HEC and ALG (1 g/L) protected the alloy by 64.13 % and 58.27 %, respectively. Two inhibitor cocktails consisting of either HEC or ALG, KI, and Date palm seed oil have been formulated. HEC- and ALG-formulations inhibited the alloy corrosion by 80.56 % and 77.43 %, respectively from EIS technique. Surface observation studies using SECM, AFM, SEM, and EDX agreed with other experimental results revealing effective corrosion inhibition by the formulations. X-ray photoelectron spectroscopy, FTIR, and UV–vis results disclose that $Mg(OH)_2$ co-existed with adsorbed inhibitor complexes.

1. Introduction

Magnesium and its alloys hold significant potential for becoming the default alternative to aluminium as structural or engineering materials due to their low density (65 % of that of aluminium), high strength, ductility, and ease of machinability. In addition, magnesium is versatile (the eighth most abundant element in the earth's crust) and non-toxic to the natural environment and human body (Esmaily et al., 2017). These endearing properties also make them materials of choice in transportation, electronics, bio-medical, and battery applications. However, the main disadvantage of magnesium and its alloys is their low corrosion resistance occasioned by their high chemical reactivity and high electron negative potential (Esmaily et al., 2017; Saji, 2019). Aqueous corrosion of Mg and its alloys with the production of hydrogen (H_2) gas occurs rapidly when exposed to salt water, moisture, or acidic environment (Saji, 2019). To ensure a profitable service life of these artefacts, their rate of corrosion has to be appreciably decreased and surface modification (coatings or inhibitors) has been proposed (Frignani, Grassi, Zanotto, & Zucchi, 2012; Saji, 2019).

There are many research papers claiming the successful mitigation of magnesium corrosion using coatings (Chen, Birbilis, & Abbott, 2011; Gray & Luan, 2002; Saji, 2019; Sviatlana, Daniel, Carsten, & Mikhail, 2017; Zhang & Wu, 2010), but such claim on the use of corrosion inhibitors particularly in chloride-rich environment is limited (Chirkunov & Zheludkevich, 2018; Lu et al., 2019). In fact, it is found that, most effective corrosion inhibitors for other metals do not work for Mg and its alloys. For example, Chirkunov and Zheludkevich (2018) tested 1,2,3-benzotriazole, 5-chloro-1,2,3-benzotriazole, and sodium dioctyl phosphate on the corrosion of Elektron WE43 Mg alloy in 0.05 M NaCl solution and found that the azoles did not inhibit the WE43 alloy corrosion. Lamaka et al. (2017) screened 151 individual compounds (organic and inorganic) for corrosion inhibition effect towards six alloys (AZ31, AZ91, AM50, WE43, ZE41 and Elektron 21) and three grades of pure magnesium and found that, only 15 exhibited inhibitive property. Of these fifteen, more than 60 % were compounds marked as toxic, carcinogenic, and harmful to the natural environment. Mei, Lamaka, Feiler, and Zheludkevich (2019) examined the influence of 53 organic bio-compounds (amino acids, antibiotics, vitamins, and saccharides) on the corrosion of CP Mg and Mg-0.8Ca alloys in chloride containing medium. It was found that 80 % of the tested compounds accelerated or minimally inhibited the degradation of the alloys. In fact, only uric acid and ascorbic acid were found to exhibit inhibition protection up to 50 % for Mg-0.8Ca alloy.

The legislation imposed by the Registration, Evaluation, Authorization, and Restriction of Chemicals (REACH) and the Paris Commission (PARCOM) on new chemicals is simple and clear: chemicals must be green compliance (Singl & Bockris, 1996; Umoren & Solomon, 2019). Greenness is defined in terms of non-bioaccumulation,

* Corresponding author.
E-mail address: umoren@kfupm.edu.sa (S.A. Umoren).

https://doi.org/10.1016/j.carbpol.2019.115466
Received 9 August 2019; Received in revised form 6 September 2019; Accepted 11 October 2019
Available online 06 December 2019

biodegradation, and zero or very low marine toxicity level (Singl & Bockris, 1996; Umoren & Solomon, 2019). The natural polymers are among the few compounds that meet the requirements of REACH and PARCOM. Besides the environmental compatibility, natural polymers are readily available hence cost-effective; possess inherent stability and multiple adsorption centers thus fulfilling one of the essential requirements for an inhibitor (Umoren & Solomon, 2019).

There are reports on starch (Bello et al., 2010), carboxymethyl cellulose (Bayol, Gürten, Dursun, & Kayakirilmaz, 2008; Umoren, Solomon, Udosoro, & Udoh, 2010), chitosan (Umoren, Banera, Alonso-Garcia, Gervasi, & Mirıfico, 2013), pectin (Umoren, Obot, Madhankumar, & Gasem, 2015), Gum Arabic (Bentrah, Rahali, & Chala, 2014; Umoren, Ogbobe, Igwe, & Ebenso, 2008), Gellan gum (Rajeswari, Kesavan, Gopiraman, & Viswanathamurth, 2013), hydroxypropyl cellulose (Mobin & Rizvi, 2016), xanthan gum (Biswas, Pal, & Udayabhanu, 2015), and dextran (Solomon, Umoren, Obot, Sorour, & Gerengi, 2018) as corrosion inhibitor for low carbon steel in acidic environment. Pectin (Fares, Maayta, & Al-Qudah, 2012) and iota carrageenan (Fares, Maayta, & Al-Mustafa, 2012) have been reported as inhibitor for aluminium in acidic environment. There is also a report on the inhibition of copper corrosion in acidic environment using chitosan (El-Haddad, 2013). Recently, we carried out a comprehensive review on the use of polymers (modified and unmodified) for the corrosion protection of industrial metals substrates (Umoren & Solomon, 2019). To the best of our knowledge, there is no information on the use of natural polymers for the corrosion protection of magnesium and its alloys. In order to fill this gap and to provide information on the anticorrosion property of natural polymers toward magnesium and its alloys, seven natural polymers namely, carboxymethyl cellulose (CMC), chitosan (CHI), pectin (PEC), Gum Arabic (GA), hydroxyethyl cellulose (HEC), alginate (ALG), and dextran (Dex) were screened for inhibition property for AZ31 Mg alloy in 3.5 wt.% NaCl solution. Their molecular structure is given in Fig. 1(a). Mass loss, gasometric, electrochemical impedance spectroscopy, and potentiodynamic polarization techniques were employed for the study. A state-of-the-art scanning electrochemical workstation utilizing localized electrochemical technique such as scanning electrochemical microscopy (SECM) was also used to probe the corrosion behavior of the Mg alloy in the absence and presence of the inhibitors. The surface of the corroded Mg alloy was examined using atomic force microscope (AFM), scanning electron microscope (SEM), Fourier-transform infrared spectroscopy (FTIR), Ultraviolet–visible spectroscopy (UV–vis), and X-ray photoelectron spectroscopy (XPS).

2. Experimental part

2.1. Materials and reagents

The metal substrate used for all experimental studies was AZ31 Mg alloy with chemical composition (wt. %) as follows: 2.5–3.5 Al, 0.6–1.4 Zn, 0.2–1.0 Mn, 0.1 Si, 0.05 Cu, and Mg as the balance (Kumar et al., 2014).

The natural polymers screened for anticorrosion property were carboxymethyl cellulose (CAS number: 9004 – 32 – 4, mol. wt.: ~ 90,000 g/mol, pH: 6.5–8.5), poly-D-galacturonic acid methyl ester from Apple (pectin) (CAS number: 9000 – 69 – 5, mol. wt.: 75,000 g/mol, degree of esterification: 65–70%), dextran from *Leuconostoc mesenteroides* (CAS number: 9004 – 54 – 0, mol. wt.: 100,000–200, 000), chitosan (CAS number: 9012 – 76 – 4, mol. wt.: 50,000–190,000 Da, viscosity: 20–30 cP, degree of deactylation: 75–85%), sodium alginate (CAS number: 9005 – 38 – 3, viscosity: 12–25 cP), hydroxyethyl cellulose (CAS number: 9004 – 62 – 0, mol. wt.: ~ 90,000 g/mol, viscosity: 75 −150 cP), and Gum Arabic from Acacia tree (CAS number: 9000 – 01 – 5, pH 4.1–4.8). They were procured from Sigma-Aldrich (Merck) and were used without further purification. All the listed natural polymers were water soluble except chitosan in which small amount of 1 % acetic acid was used for complete dissolution. Sodium chloride salt and potassium iodide also used in the investigation were equally purchased from Sigma-Aldrich. Date palm seeds were removed from edible date palm fruit obtained from the King Fahd University campus shopping mall, dried, powdered and the oil extracted using Soxhlet extractor with n-hexane.

2.2. Solution and sample preparation

A sheet of AZ31 Mg alloy was machined into experimental samples of 2.022 cm × 2.089 cm × 0.395 cm as dimension. The samples were mechanically wet abraded with emery paper of #600, #800, and #1000 grits. They were washed in distilled water, rinsed in acetone, and dried using a Buchler Torramet specimen dryer.

The corrodent (3.5 wt% NaCl) was prepared by dissolving an appropriate amount of NaCl salt in distilled water. For anticorrosion property screening, 1 g each of the natural polymers was added to 1000 cm^3 of the corrodent. Where the effect of concentration was considered, 0.5, 1.0, and 2.0 g/L were chosen. The inhibitor cocktail was formulated from either HEC or ALG (1 g/L), potassium iodide (0.25 g/L), and Date palm seeds oil (0.5 g/L).

2.3. Mass loss experiments

Five 150 mL capacity bottles labeled blank, HEC, ALG, HEC-formulation, and ALG-formulation were filled with 100 mL of the respective solutions. Two prepared samples whose initial weight have be measured were freely suspended with the aid of a thread in each of the bottles. The reaction bottles were allowed to stand at room temperature for 24 h. Thereafter, the specimens were retrieved, cleaned following the ASTM-G1–03 (2017) procedure, dried using specimen dryer, and reweighed. The mean mass loss ($\bar{m}$) was calculated and used in the computation of the corrosion rate (v) according to the following equation (ASTM-G1–03, 2017):

$$v\ (\text{mm/yr}) = \frac{8.76 \times 10^4 \times \bar{m}}{A \times t \times d} \quad (1)$$

where t is the immersion time (h), d is the density (g/cm^3) and A is the surface area (cm^2) calculated using the equation (NACE Standard Test Method TM0193, 2016):

$$A = 2(wl + dl + dw) \quad (2)$$

where w = width (cm); d = thickness (cm); and l = length (cm). The inhibition efficiency (η_{WL}, %) of the inhibitors from the mass loss technique was calculated using Eq. (3).

$$\eta_{WL} = \frac{W_0 - W}{W_0} \times 100 \quad (3)$$

where W_0 and W are the mean mass losses of the samples in the uninhibited and inhibited systems respectively.

2.4. Gasometric experiments

Magnesium is a very reactive metal, degrading in an unprecedented rate in acidic and halide containing media (Saji, 2019). The overall degradation reaction can be represented as (Saji, 2019):

$$Mg\ (s) + 2H_2O\ (l) \rightarrow Mg(OH)_2\ (aq) + H_2\ (g) \quad (4)$$

The hydrogen gas liberated can be used as an indicator of the rate of degradation (Saji, 2019). In addition, oxygen reduction reaction can occur as a secondary cathodic reaction (Lamaka et al., 2017); because our experimental set-up (the schematic diagram can be found in our previous publication (Kumar, Hassan, Sorour, Paramsothy, & Gupta, 2019) cannot impede oxygen access, we have adopted the name 'gasometric' instead of hydrogen evolution. The rate of degradation of AZ31 Mg alloy exposed to 3.5 wt% NaCl solution without and with

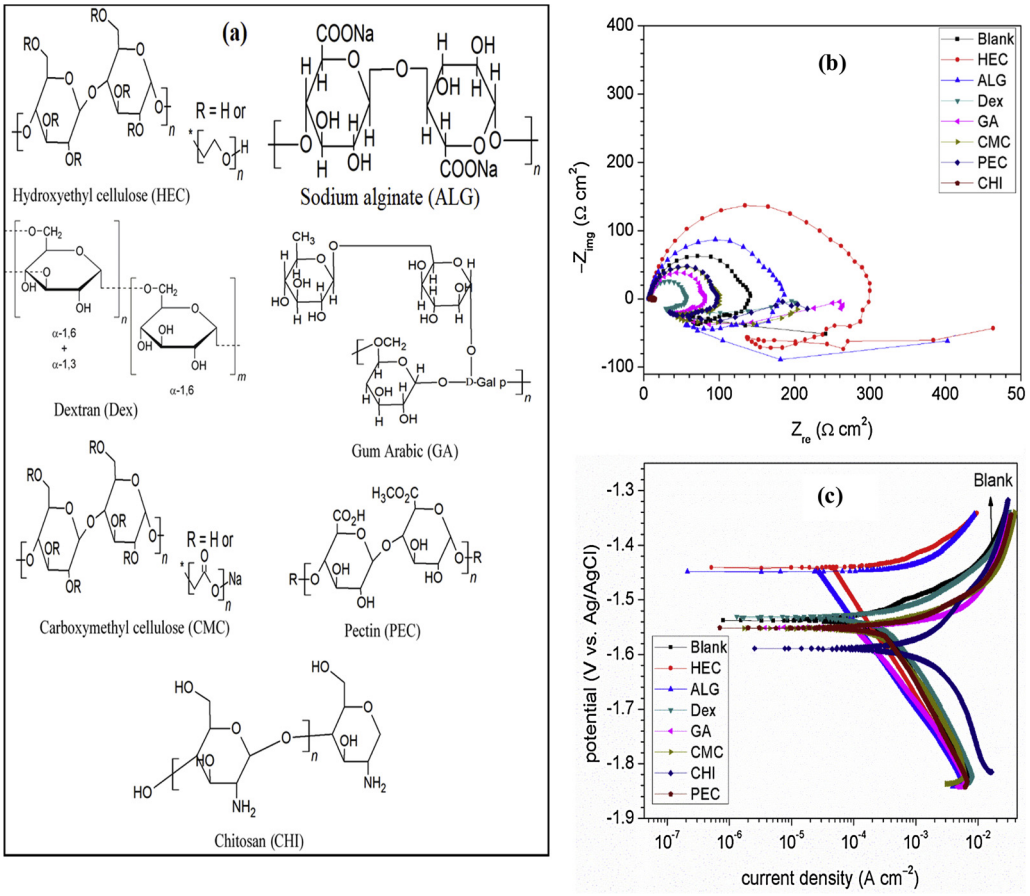

Fig. 1. (a) Chemical structure of natural polymers studied; (b) electrochemical impedance spectra, and (c) potentiodynamic polarization graphs of AZ31 Mg alloy in 3.5 wt.% NaCl solution without and with the various natural polymers.

additives was studied by monitoring the volume of gas liberated at 2 h interval for 24 h. The degradation rate (v_d, cm^3 h^{-1}) was computed using the equation (Umoren, Solomon, Udosoro, & Udoh, 2010):

$$v_d = \frac{V_t - V_i}{t_t - t_i} \quad (5)$$

where V_t and V_i are the volumes of gas liberated at time t_t and t_i, respectively.

2.5. Electrochemical experiments

A Gamry Potentiostat/Galvanostat/ZRA Reference 600 instrument was employed for the electrochemical impedance spectroscopy (EIS) and the potentiodynamic polarization (PDP) experiments. The electrochemical set-up comprised of the prepared AZ31 Mg alloy sample as the working electrode, a graphite rod as the counter electrode, and a silver/silver chloride (Ag/AgCl) as the reference electrode. To establish at least a pseudo steady state condition, OCP measurement was performed for 1800s before commencing EIS experiments. The EIS tests were conducted between the initial frequency of 100,000 Hz and final frequency of 0.01 Hz, with acquirement of 10 points/decade and a signal amplitude of 10 mV at open circuit potential (E_{ocp}). The PDP experiments were carried out at the potential of ± 0.25 V versus E_{ocp} using a scan rate of 0.2 mVs^{-1}. The analysis of EIS and PDP data was done using Echem analyst and EC-lab software, respectively.

2.6. SEM, EDX, AFM, XPS, FTIR, UV–vis, and SECM experiments

The morphologies of the surfaces of AZ31 Mg alloy specimens before and after immersion in 3.5 wt.% NaCl solutions without and with the additives for 24 h and the elemental composition of the products on the surfaces were determined using a Scanning Electron Microscope (SEM) JEOL JSM-6610 LV coupled with an energy dispersive X-ray spectroscopy. The roughness characteristics of the exposed surfaces were studied utilizing a 5420 atomic force microscope (N9498S, Agilent Technologies, UK) operated in the contact mode under ambient conditions. Xray photoelectron spectroscopy (XPS) studies were performed utilizing ESCALAB 250Xi XPS spectrometer with a monochromatic Al Kα Xray source. The XPS data were analyzed using Avantage v5,51,0,5371 software.

The ATR-FTIR analysis was performed for pure HEC or ALG and the films extracted from the Mg alloy surface immersed in 3.5 wt.% NaCl solution containing HEC or ALG for 24 h at 25 °C. The ATR-FTIR spectra were recorded in the range of 500–4000 cm^{-1} utilizing a FTIR spectrophotometer (TA instrument with universal ATR attachment, Nicolet iS5, Thermo Scientific). A JASCO770 UV–Vis spectrophotometer was used to record the UV–vis spectra of 3.5 wt.% NaCl solution devoid of and containing HEC or ALG after 24 h of immersing a AZ31 Mg alloy sample. The UV–vis scanning was performed in the range of 200–800 nm using a dual beam operated at a resolution of 1 nm with a scan rate of 200 nm/min.

The SECM measurements were performed using M370 scanning electrochemical workstation. An SECM ultra-microelectrode (UME) with a platinum tip of 10 µm as the diameter was used as working electrode. The counter and reference electrodes used were as mentioned in Section 2.5. An area of 500 × 500 µm was examined and the scan rate was 25 µm/s. The substrate-UME tip distance was first fixed at a constant distance with the aid of a digital microscope and then adjusted to 50 µm. Substrate generation/Tip collection at SECM mode was utilized in analyzing the gas evolution at the Mg alloy surface by applying

Table 1
The individual influence of some natural polymers on the corrosion of AZ31 Mg alloy in 3.5 wt.% NaCl solution at ordinary temperature. (Red background color means the compound accelerates corrosion, η < 0 %; Green color means moderate inhibition effect, η > 40 %).

S/N	System/polymer studied	Derived parameters					
		EIS technique		PDP technique		Mass loss technique	
		R_{pEIS} (Ω cm^2)	η_{EIS} (%)	R_{pPDP} (Ω cm^2)×10^{-3}	η_{PDP} (%)	Mass loss (g)	η_{WL} (%)
1	Blank (3.5 wt.% NaCl)	53.01±0.13	-	45.52	-	0.0046±0.01	-
2	Dextran	31.61±0.45	- 67.67	28.75	-58.31	0.0069±0.01	-50.00
3	Gum Arabic	36.28±1.32	- 46.09	30.79	-47.83	0.0066±0.00	-43.48
4	Carboxymethyl cellulose	43.10±0.79	- 23.00	36.26	-25.54	0.0056±0.01	-21.74
5	Hydroxylethyl cellulose	147.80±2.35	64.13	124.06	63.30	0.0017±0.00	63.04
6	Pectin	38.25±0.21	- 38.59	33.28	-36.77	0.0062±0.00	-34.78
7	Sodium alginate	127.04±1.13	58.27	103.39	55.97	0.0020±0.01	56.52
8	Chitosan	26.53±0.16	- 99. 82	22.78	-99.79	0.4632±0.01	-99.70

the UME tip potential of 0.0 V vs Ref. At this tip potential, the gas released at the cathodic sites is rapidly oxidized at a UME tip ($H_2 \rightarrow 2H^+ + 2e^-$) (Salleh, Thomas, Yuwono, Venkatesan, & Birbilis, 2015). Since this reaction is diffusion controlled, the current measured at the UME tip is a direct measure of the local gaseous concentration. Based on previous report (Salleh et al., 2015), 1 cm^2 was selected as the exposure area to avoid excessive signal noise due to vigorous gas bubbles and the accumulation of protons rising from the gas oxidation at the UME.

3. Results and discussion

3.1. Anticorrosion property screening

Seven natural polymers (HEC, ALG, CMC, Dex, GA, CHI, and PEC) were screened for anticorrosion property towards AZ31 Mg alloy in 3.5 wt.% NaCl solution using EIS, PDP, and weight loss techniques. The results obtained are given in Fig. 1(b & c) and in Table 1. Generally, the EIS spectra in Fig. 1(b) exhibit two capacitive loops at high and medium frequencies and an inductive loop at low frequencies. The capacitive loops at high frequencies are associated with the charge transfer and corrosion products/adsorbed inhibitor films resistances while the middle capacitive loop is due to the diffusion processes through the layer (Frignani et al., 2012). The inductive loop is linked to the relaxation of the adsorbed corrosion products/inhibitor films (Solmaz, Kardas, ulha, Yazıcı, & Erbil, 2008). Two branches denoting the cathodic and the anodic half reactions characterize the PDP graph in Fig. 1(c). The EIS spectra for CMC, Dex, GA, CHI, and PEC were modeled using the equivalent circuit (EC) inserted in Fig. S1(a) of the supplementary information which had been recently used by Nabizadeh, Sarabi, and Eivaz Mohammadloo, (2019)) for the same purpose. Similarly, the impedance spectra for the blank, HEC and ALG were fitted using the EC inserted in Fig. S1(b). King, Birbilis, & Scully (2014) had used it for the analysis of pure Mg impedance spectra recorded in NaCl solution. For the EC in Fig. S1(a), the charge transfer resistance (R_{ct}) and the inductive resistance (R_L) are in parallel arrangement. The R_{ct} and the film resistance (R_f) are in series connection but in parallel connection to the R_L in the EC in Fig. S1(b). The frequency dependent impedance response of the entire EC in Fig. S1(a) and (b) can be described by simple circuit analysis given in Eqs. 6 & 7, respectively. This allows the simplification of the polarization resistance (R_p) using Eqs. (8) and (9).

$$/Z/=Z_{R_s} + \left(\frac{1}{Z_Q} + \frac{1}{Z_{R_L} + Z_L} + \frac{1}{Z_{R_{ct}}}\right)^{-1} \quad (6)$$

$$/Z/=Z_{R_s} + \left(\frac{1}{Z_{C_1}} + \frac{1}{Z_{R_{ct}} + \left(\frac{1}{Z_{C_2} + Z_{R_f}}\right)^{-1}} + \frac{1}{Z_{R_L} + Z_L}\right)^{-1} \quad (7)$$

$$\frac{1}{R_p} = \frac{1}{R_{ct}} + \frac{1}{R_L} \quad (8)$$

$$\frac{1}{R_p} = \frac{1}{R_{ct} + R_f} + \frac{1}{R_L} \quad (9)$$

The representative fitted graphs are shown in Fig. S1(a–c). The inhibition efficiency (η(%)) was calculated following Eq. (10). The calculated values of R_p and η_{EIS} are listed in Table 1. The PDP curves were extrapolated using an EC-lab software (Fig. S1(b)). The Stern-Geary equation (Eq. (11)) was used for the computation of the polarization resistance for this technique. The values of the R_{pPDP} and η_{PDP} are also presented in Table 1.

$$\eta(\%) = \left(\frac{R_{p(1)} - R_{p(0)}}{R_{p(1)}}\right) \times 100 \quad (10)$$

$$i_{corr} = \frac{\beta_a \beta_c}{2.303 R_p (\beta_a + \beta_c)} \quad (11)$$

where $R_{p(0)}$ and $R_{p(1)}$ are the polarization resistances in the absence and presence of the additives, respectively; i_{corr} is the corrosion current density, β_a and β_c are the anodic and cathodic slopes, respectively.

The inspection of Fig. 1(b & c) and Table 1 reveal that, exception of HEC and ALG, the other natural polymers accelerated the corrosion of the Mg alloy in the studied corrosive medium. Chitosan has the highest corrosion accelerating effect (almost 100 %). The reason for the accelerating effect of these polymers is not fully understood. However, natural polymers have been reported as chelating agents for di- and trivalent cations and chitosan is claimed to have the highest chelating ability in comparison with other natural polymers (Crini, Morin-Crini, Fatin-Rouge, De´on, & Fievet, 2017; Zalloum & Mubarak, 2013). It could be that, in the studied medium, the polymers formed chelates with Mg^{2+} ions. In the case of CMC, Dex, GA, CHI, and PEC, the Mg-polymer chelates may have formed in the electrolyte rather than on the Mg surface and this accelerated the corrosion of the alloy. Similar explanation was given by Lamaka et al. (2017) on the corrosion accelerating effect of 8-hydroxyquinoline towards Al-containing Mg alloy in 0.5 wt.% NaCl solution. Additionally, the acetic acid used in dissolving chitosan may have also contributed to the observed high corrosion accelerating effect.

Based on the results of the screening experiments (Fig. 1(b & c), Table 1), HEC and ALG were selected for elaborate studies. The results in Table 1 show that, HEC and ALG inhibited the AZ31 Mg alloy corrosion in 3.5 wt.% NaCl solution by 64.13 % and 58.27 % (from EIS technique), respectively. It was necessary to investigate the influence of concentration on the performance of HEC and ALG. The concentrations of the polymers considered in this set of experiments were 0.5 g/L, 1 g/L and 2 g/L. Fig. 2 shows the electrochemical characteristics of AZ31 Mg alloy in 3.5 wt.% NaCl solution without and with different concentrations of (a, c) ALG and (b, d) HEC at ordinary temperature. The corresponding electrochemical parameters derived from the analysis of the electrochemical data are presented in Tables 2 and 3. The

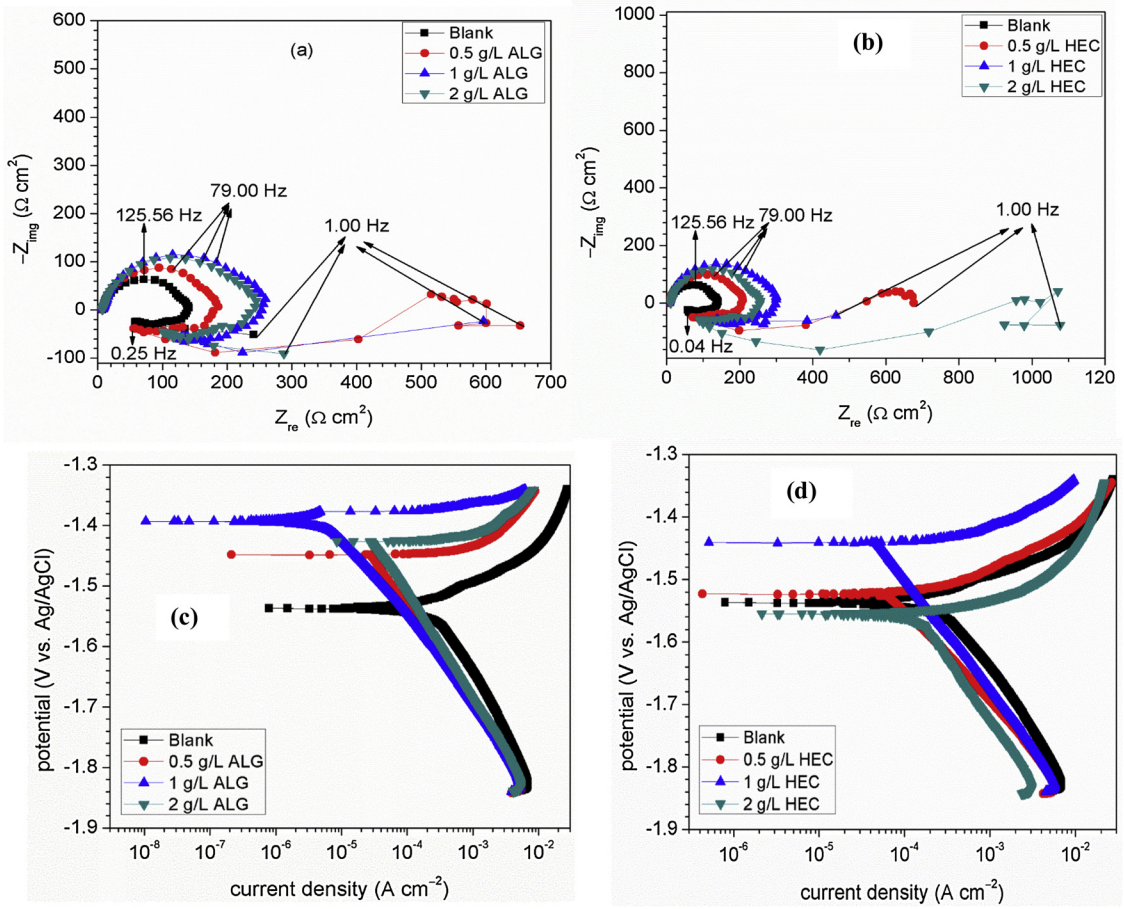

Fig. 2. Electrochemical characteristics of AZ31 Mg alloy in 3.5 wt.% NaCl solution without and with various concentrations of (a, c) ALG and (b, d) HEC at ordinary temperature.

two natural polymers behaved alike although HEC demonstrated better corrosion inhibition performance than ALG. It is observed that, the polarization resistance (Tables 2 and 3) increased as the concentration of the polymer was raised from 0.5 g to 1.0 g but declined with further increment. The inhibition efficiency behaves in similar manner. That is, the best inhibition performance was achieved with the 1.0 g of the polymers. It could be argued that, in 3.5 wt.% NaCl solution containing 0.5 g of the polymers, the concentration of the inhibitors was not sufficient for significant adsorption. As the concentration was increased to 1.0 g, more inhibitor molecules were available for adsorption and this resulted in larger surface coverage and better corrosion inhibition (Tables 2 and 3). The solution may have been saturated when 2.0 g of the polymers was added such that, the distance between individual molecules became too close resulting in molecules aggregation. Again, the adsorbed molecules could interact with the un-adsorbed molecules and cause the detachment of the adsorbed species from the substrate surface. This exposed some areas on the surface to fresh corrosive attack and caused the observed decline in inhibition performance. Similar argument can be found in the corrosion literature (Pavithra, Venkatesha, Vathsals, & Nayana, 2010; Umoren, Solomon, Ali, & Dafalla, 2019).

It is worthy to point out the remarkably low values of the anodic slope (β_a) relative to those of the cathodic slope (β_c). For instance, the β_a value for the blank is 14.00 mV dec^{-1} whereas the β_c value is 149.40 mV dec^{-1} (Table 3). This is due to the fact that, magnesium is non-polarizable anodically (King et al., 2014). Normally, the value of β_a should be $\leq$150 mV dec^{-1} while the value of β_c should be in the vicinity of $\sim 200-300$ mV dec^{-1} (Cao et al., 2013; King et al., 2014; Qiao, Shi, Hort, Abidin, & Atrens, 2012). The R_p is therefore an important parameter that must be considered during magnesium corrosion and inhibition studies. In this work, the inhibition performance was determined using this very important parameter and its determination was done using the Stern-Geary equation given herein as Eq. (11). The values of the instantaneous corrosion rate (v) also given in Table 3 was calculated using Eq. (12) (Cao et al., 2013). As could be seen in the table, the degradation rate of the alloy was slower in the salt solution containing the natural polymers than in their absence.

$$v = 22.85 \times i_{corr} \quad (12)$$

The corrosion inhibition afforded by the optimum concentration of the polymers (1 g/L) is moderate (Tables 2 and 3). For ALG, the inhibition efficiency is in the range of 56–58% while that of HEC is between 63–64%. KI and Date palm seeds oil studied independently inhibited AZ31 Mg alloy in 3.5 wt.% NaCl solution by 31.70 % and 10.70 % (Table 2). In real application, a single compound can rarely provide the desire corrosion protection, as such commercial inhibitor is usually a cocktail (also called formulation or package) of several components (Finšgar & Jackson, 2014). A formulation consisting of HEC or ALG, KI, and Date palm seeds oil was developed and tested against the corrosion of AZ31 Mg alloy in 3.5 wt.% NaCl solution. Fig. 3(a) & (b) show the comparative electrochemical impedance spectra of the formulations with the polymers (HEC and ALG), KI, and Date palm seed oil. Clearly, the semicircles at higher frequencies for the polymer-formulations are remarkably larger compared to that of independent components. This infers better retardation of the alloy degradation in the corrosive solutions containing the formulations than in the solutions containing the individual components. It suggests a co-adsorption in the systems containing the formulations. A substantial amount of the inhibitor

Table 2
Results of fitting analysis from electrochemical impedance measurements of AZ31 Mg alloy in 3.5 wt.% NaCl solution without and with various additives at ordinary temperature.

System	Derived parameters								Calculated parameters	
	R_s (Ω cm^2)	C_1 (μF cm^{-2})	R_{ct} (Ω cm^2)	R_f (Ω cm^2)	L (Ω s cm^2)	R_L (Ω cm^2)	C_2 (μF cm^{-2})	$x^2 \times 10^{-3}$	R_{pEIS} (Ω cm^2)	η_{EIS} (%)
Blank	8.08 ± 0.07	12.09 ± 0.00	122.60 ± 2.77	0.90 ± 0.08	82.01 ± 2.74	92.87 ± 2.21	4.49 ± 0.03	35.03	53.01 ± 0.13	–
0.5 g/L ALG	6.80 ± 0.07	7.58 ± 0.00	175.60 ± 2.91	18.16 ± 2.55	40.76 ± 1.11	156.30 ± 2.68	4.82 ± 0.00	126.40	86.51 ± 1.32	38.73
1 g/L ALG	7.98 ± 0.07	8.11 ± 0.00	201.20 ± 6.16	49.18 ± 6.10	133.50 ± 5.19	257.90 ± 6.01	61.24 ± 0.00	39.31	127.04 ± 3.05	58.27
2 g/L ALG	7.87 ± 0.07	9.18 ± 0.00	215.40 ± 1.67	19.51 ± 5.01	134.20 ± 4.39	178.60 ± 4.78	4.13 ± 0.00	33.95	101.46 ± 2.46	47.75
0.25 g/L KI	7.45 ± 0.62	10.21 ± 0.00	220.80 ± 1.99	1.64 ± 0.64	44.19 ± 1.17	120.30 + 2.89	1.54 ± 0.00	80.33	77.60 ± 1.03	31.70
0.5 g/L Date palm seed oil	6.26 ± 0.53	13.68 ± 0.00	144.70 ± 1.37	4.51 ± 1.20	17.80 ± 6.32	101.40 + 2.09	1.91 ± 1.51	40.20	59.40 ± 1.06	10.70
ALG-formulations	18.06 ± 0.15	19.97 ± 0.00	469.60 ± 2.95	20.32 ± 4.56	66.90 ± 3.10	451.30 ± 2.33	99.30 ± 0.00	92.38	234.91 ± 1.56	77.43
0.5 g/L HEC	6.67 ± 0.08	5.85 ± 0.00	183.20 ± 2.45	12.03 ± 1.84	52.75 ± 1.73	163.20 ± 4.28	4.53 ± 0.00	119.90	88.89 ± 1.32	40.37
1 g/L HEC	6.92 ± 0.06	7.37 ± 0.00	262.30 ± 4.58	25.26 ± 4.94	163.80 ± 7.19	304.10 ± 7.33	341.10 ± 0.00	37.54	147.80 ± 2.97	64.13
2 g/L HEC	10.60 ± 0.13	3.39 ± 0.00	222.20 ± 2.35	10.63 ± 1.36	75.56 ± 2.33	174.30 ± 4.85	4.08 ± 0.00	117.70	99.68 ± 1.14	46.82
HEC-formulations	33.05 ± 0.25	7.32 ± 0.00	538.80 ± 4.80	23.82 ± 7.56	186.30 ± 3.13	529.00 ± 4.51	102.40 ± 0.06	78.18	272.65 ± 2.86	80.56

molecules may have been adsorbed on the alloy surface, blocked the charge transfer path, and prolonged the completion of corrosion reaction cycle resulting in the observed larger impedance (Fig. 3(a & b)). The analysis of all the impedance data in Fig. 3(a & b) were done with the EC inserted in Fig. S1(b). The derived and calculated parameters are presented in Table 2. The polarization resistance of the alloy in the formulations containing systems was almost double the polarization resistance in the solutions containing the natural polymers. For instance, the R_{pEIS} for the alloy in 1 g/L ALG containing solution was 127.04 ± 3.05 Ω cm^2 and the corresponding inhibition efficiency was 58.27 %. Similarly, in HEC containing system, the R_{pEIS} was 147.80 ± 2.97 Ω cm^2 corresponding to inhibition efficiency of 64.13 %. However, in the systems containing the ALG- and HEC-formulations, the R_{pEIS} was 234.91 ± 1.56 Ω cm^2 and 272.65 ± 2.86 Ω cm^2 and the protection efficiency was 77.43 % and 80.56 %, respectively.

Fig. 3(c) displays the potentiodynamic polarization curves for AZ31 Mg alloy in 3.5 wt.% NaCl solution without and with different additives. The polarization parameters derived from the extrapolation of the linear segments of the curves as well as the calculated parameters are given in Table 3. It is clearly seen in Fig. 3(c) that both the anodic and cathodic polarization curves are displayed toward lower values when polymer-formulations was present than when the natural polymers alone were added. This point to better corrosion protection of the alloys by the formulation than the individual natural polymers. It is deduced from Fig. 3(c) that, the natural polymers and their formulations retarded both the anodic and cathodic corrosion reactions, although the dominant effect seems to be on the anodic part. The inhibition efficiency value for ALG and HEC from the PDP technique is 55.97 % and 63.30 %, respectively and that of the ALG- and HEC-formulations is 80.62 % and 85.34 %, respectively and are in good agreement with the values from EIS experiments (Table 2).

The bar chart showing the corrosion rate (v) of AZ31 Mg alloy in 3.5 wt.% solution devoid of and containing either HEC, ALG, HEC-formulation, or ALG-formulation at 25 °C obtained from mass loss technique is shown in Fig. 3(d). The corrosion rate is higher in the blank solution than in the inhibited systems. The formulations perform better than the polymers alone. In this technique, inhibition efficiency up to 80.43 % was achieved for HEC-formulation while that of ALG-formulation is 78.26 %, and compares well with the electrochemical results.

Fig. 3(e) shows the variation of the volume of H_2 gas evolved with time during the corrosion of AZ31 Mg alloy in 3.5 wt.% solution devoid of and containing inhibitors at normal temperature. A linear relationship between the volume of gas evolved and immersion time is observed in the plot. Similar observation has been reported (Cao et al., 2013; Umoren et al., 2010a). As should be expected, there was rapid and abundant gas evolution in the unprotected NaCl solution. The results reveal that, the rate of gas evolution was 1.06 mL cm^{-2} h^{-1} in the blank solution. The corrosion inhibition property of HEC and ALG is also obvious in Fig. 3(e). The evolution of gas in the systems inhibited with the natural polymers was lesser compared to that of the blank. The presence of HEC and ALG in the corrosive medium decreased the rate of gas evolution from 1.06 mL cm^{-2} h^{-1} to 0.38 mL cm^{-2} h^{-1} and 0.65 mL cm^{-2} h^{-1}, respectively.

This corresponded to protection efficiency of 63.95 % and 39.18 %, respectively. Again, a superior suppression of the alloy degradation was achieved with the formulations. There was a remarkable decline in the volume of gas liberated from the alloy surface in the NaCl solution containing the formulations. For the system containing ALG-formulation, the rate of gas evolution was 0.25 mL cm^{-2} h^{-1} relative to 0.65 mL cm^{-2} h^{-1} in ALG containing system. The level of protection achieved with the formulation was 76.18 %. Similarly, the HEC-formulation suppressed the rate of gas liberation and maintained the rate at 0.20 mL cm^{-2} h^{-1}; this corresponded to protection efficiency of 81.19 %. There is agreement between the mass loss (Fig. 3(d), gasometric (Fig. 3(e), and the electrochemical (Tables 2 and 3) results.

Table 3
Results of fitting analysis from potentiodynamic polarization measurements of AZ31 Mg alloy in 3.5 wt.% NaCl solution without and with various additives at ordinary temperature.

System	Derived parameters					Calculated parameters	
	$-E_{corr}$ (mV vs. Ag/AgCl)	i_{corr} (μA cm^{-2})	β_a (mV dec^{-1})	β_c (mV dec^{-1})	V (mm yr^{-1})	R_{pPDP} (Ω cm^2) × 10^{-3}	η_{PDP} (%)
Blank	1551.23	122.09	14.00	149.40	2.79	45.52	–
0.5 g/L ALG	1427.50	32.28	5.70	175.50	0.74	74.26	38.69
1 g/L ALG	1441.82	30.14	7.50	166.60	0.69	103.39	55.97
2 g/L ALG	1456.52	38.43	7.60	160.10	0.88	81.98	44.47
ALG-formulation	1393.02	21.69	12.90	130.20	0.50	234.95	80.62
0.5 g/L HEC	1555.83	30.72	5.90	194.90	0.70	80.95	43.76
1 g/L HEC	1524.35	75.87	25.30	151.60	1.73	124.06	63.30
2 g/L HEC	1450.88	27.60	6.50	156.30	0.63	98.18	53.63
HEC-formulation	1473.78	16.37	12.90	126.60	0.37	310.61	85.34

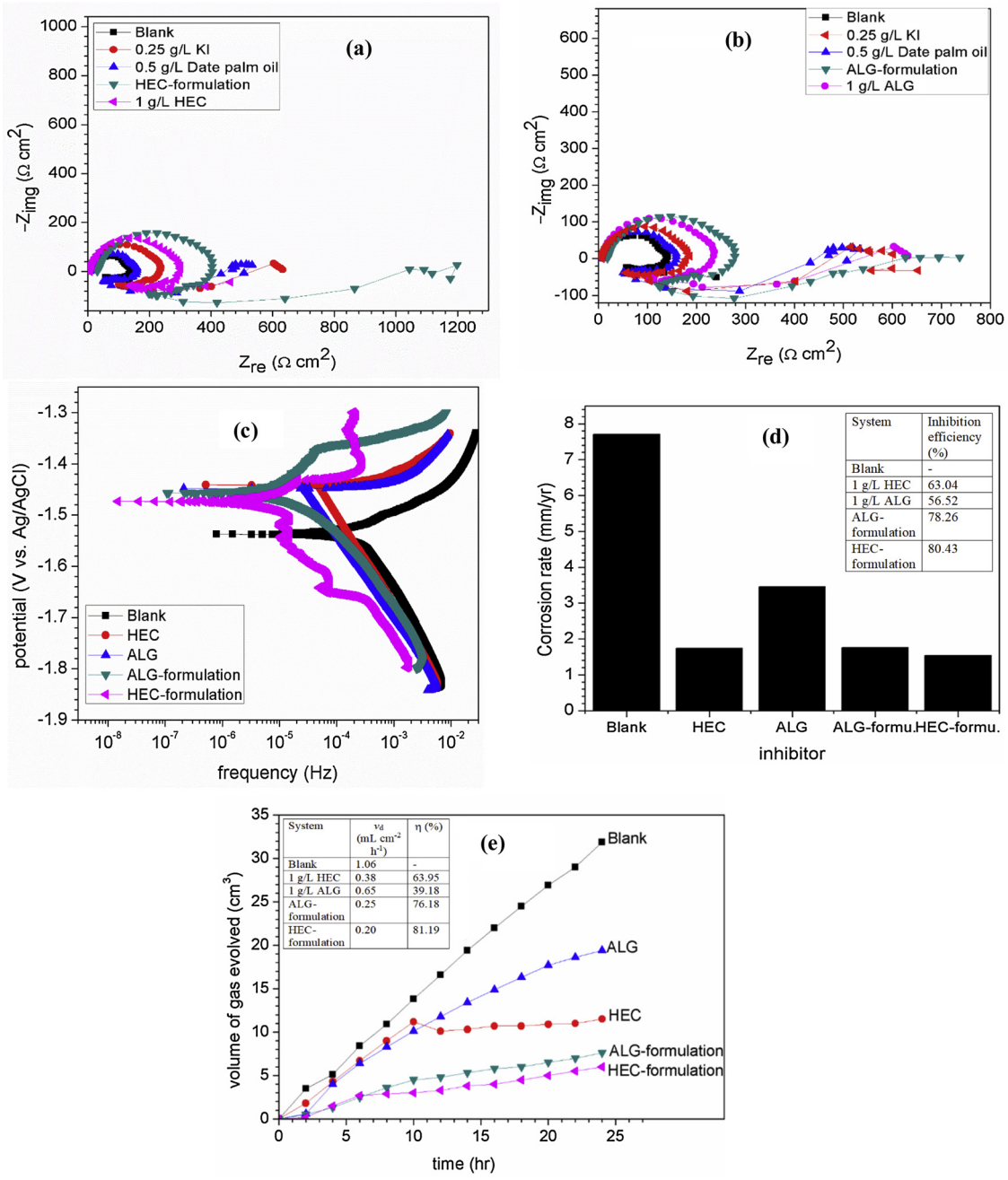

Fig. 3. (a, b) Electrochemical impedance spectra, (c) potentiodynamic polarization curves, (d) corrosion rate chart, and (e) variation of hydrogen evolution with time for AZ31 Mg alloy in 3.5 wt.% NaCl solution without and with various additives.

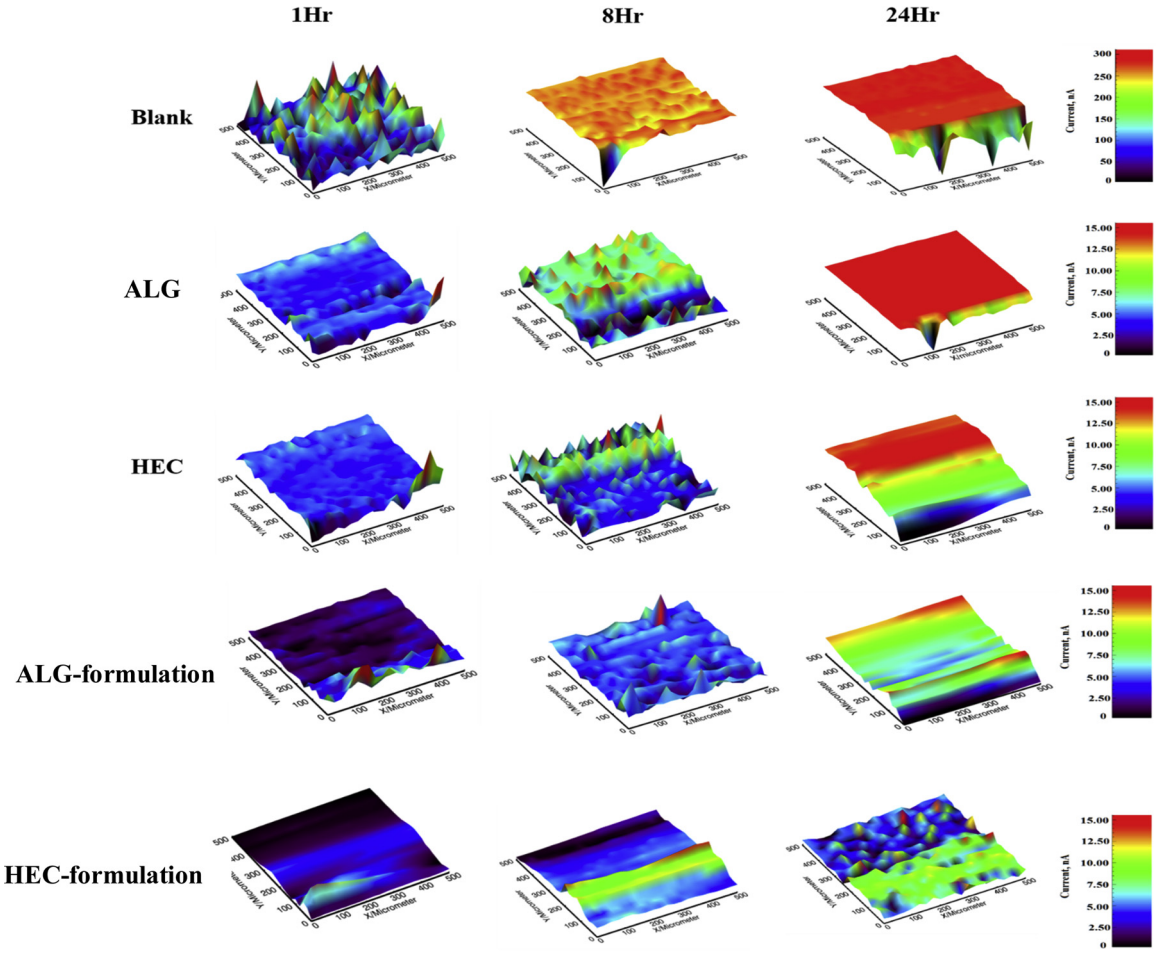

Fig. 4. SECM mapping images of AZ 31 Mg substrates with and without inhibitor as function of immersion time.

3.2. Surface observation investigations

3.2.1. SECM studies

In comparison with the conventional electrochemical techniques, SECM has some merits, which includes high spatial resolution, low iR drop, and multiple modes of operation. In recent years, SECM has been utilized in evaluating the gas evolution reactions on the surface of Mg and its alloys through substrate generation/tip collection mode (Jamali, Moulton, Tallman, Forsyth, Weber, Mirabedini et al., 2015; Jamali, Moulton, Tallman, Forsyth, Weber, Wallace, 2015; Mena-Morcillo, Veleva, & Wipf, 2018). The evolution of H_2 at the substrate surface and the consumption of H_2 at the UME tip can be recorded through the generator–collector mode. The variation in the magnitude of current measured at UME tip is a sign of different amount of hydrogen evolution from the substrate surface. However, the SECM mapping images of bare AZ31 Mg substrates are not indicative of a distinguished localized behavior due to the vigorous diffusion of more H_2 gas towards the UME tip in longer immersion time.

Fig. 4 displays the SECM mapping results in substrate generation/tip collection mode for sensing the gas released at the surface of AZ31 Mg alloy substrate in NaCl solutions without and with inhibitors. It is well established that the main regions of H_2 evolution are where the dissolution/corrosion process of Mg occur vigorously and the local pH is extremely alkaline (Jamali et al., 2014). As seen in Fig. 4, the AZ31 Mg alloy in the blank solution exhibited higher level of H_2 evolution as reflected by the higher tip current, which is indicative of an intense corrosion process at the alloy surface. The regions displaying higher tip current are the regions experiencing larger evolution of H_2 gas, and hence there was more severe corrosion taking place in the regions. Moreover, the value of the tip current was increased with increase in the immersion time, signifying the severity of corrosion at the Mg surface. It is clear from Fig. 4 that the tip current on the entire scan surface of the blank substrate surface showed a large fluctuation and the maximum value of 300 nA was found after 24 h of immersion. Compared with the blank solution, observable variances as specified by the magnitude of the tip current are detected with the addition of ALG and HEC. The SECM maps of these samples seemed to be more homogeneous than the blank substrate. Moreover, compared with the AZ31 alloy surface in the uninhibited system, the inhibited surfaces showed lower values of tip current (0 − 15 nA) even after 24 h of immersion, demonstrating lower corrosion rate on these surfaces in NaCl solution. In particular, the tip current for the alloy when exposed to ALG- and HEC-formulations is found to be much lesser compared to that of ALG and HEC samples. This again demonstrates the effectiveness of the formulations in suppression of the degradation of the alloy in the studied medium. It is interesting to note from this technique that HEC and HEC-formulation were better inhibitors than ALG and ALG-formulations. For instance, the mapped images for HEC and HEC-formulation show that, even after 24 h, the tip current was still in the blue region whereas, the mapped image for ALG is more like that of the blank at 24 h.

In order to validate the significant reduction of hydrogen evolution reaction by the addition of investigated inhibitors, the values of normalized UME tip current was plotted against the function of immersion period (Fig. S2). A close inspection of the plots disclose that, the tip current significantly decreased during the first few hours of immersion, and then increased slightly as immersion period prolonged. This validate the adsorption and formation of thin inhibitor film with respect to

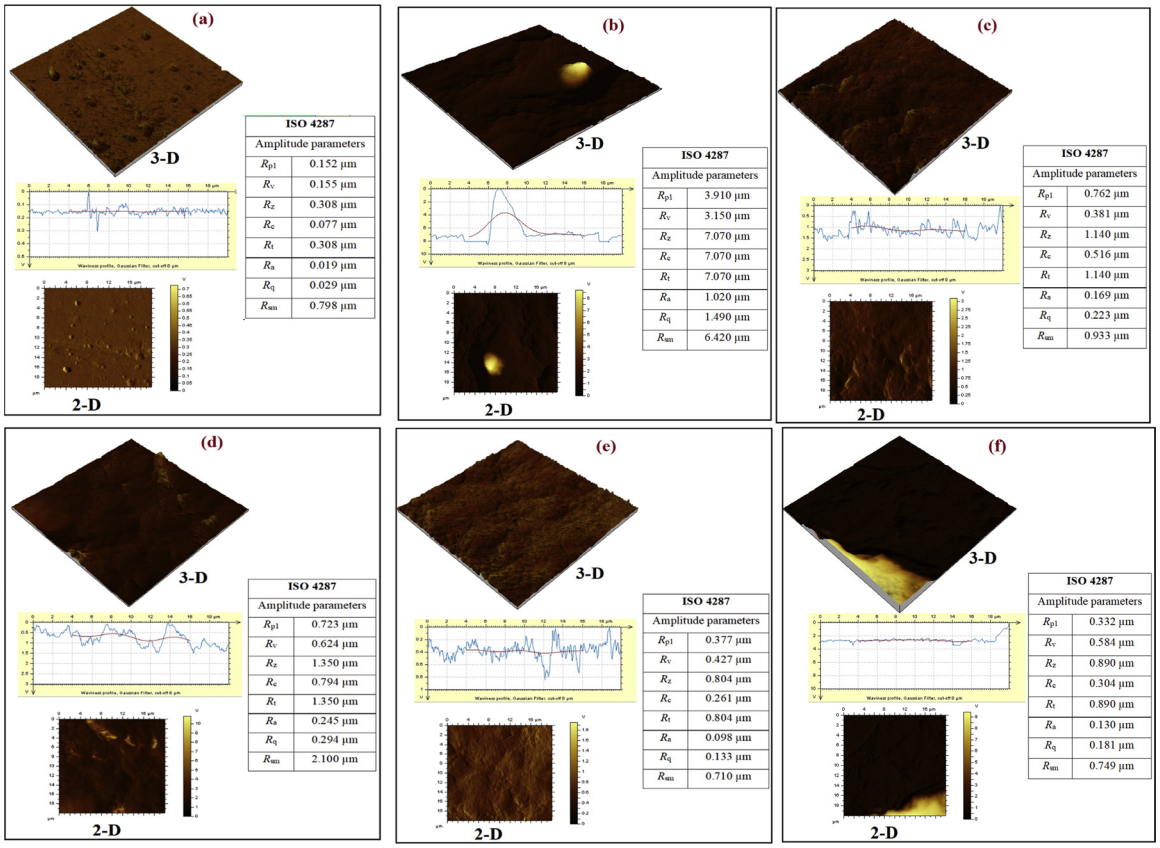

Fig. 5. AFM images in 2-D and 3-D formats for AZ31 Mg alloy after (a) mechanical abrasion and immersion in 3.5 wt.% NaCl solution (b) without and with (c) HEC, (d) ALG, (e) HEC-formulation, (f) ALG-formulation for 24 h under normal atmospheric condition.

exposure time. It can be concluded from the SECM results (Fig. 4; Fig. S2) that the addition of the natural polymers especially their formulations effectively retarded the dissolution of AZ31 Mg alloy in 3.5 wt.% NaCl solution by adsorption and formation of protective films on the alloy surface. The SECM results are in perfect agreement with the chemical (Fig. 3(c & d)) and electrochemical results (Tables 2 and 3).

3.2.2. AFM studies

The surface texture of AZ31 Mg alloy samples was studied using the atomic force microscope. Fig. 5 shows typical AFM images of AZ31 Mg alloy (a) after mechanical abrasion and after immersion in 3.5 wt.% NaCl solution (b) without inhibitor, and with (c) HEC, (d) ALG, (e) HEC-formulation, (f) ALG-formulation for 24 h under normal atmospheric condition. One of the texture profiles currently defined by the International Organization of Standardization (ISO) is the roughness profile (ISO 4287), which list certain parameters for the evaluation of surface roughness (EN ISO 4287, 1998; Mitutoyo Corporation, 2014; Solomon, Gerengi, & Umoren, 2017). Some of them are R_p[1] (maximum peak height), R_v (the maximum valley depth), R_z (the average peak to valley height), and R_c (the average peak to valley height with no limit to the amount of bands and valleys) (EN ISO 4287, 1998; Mitutoyo Corporation, 2014). Others include R_t (the largest peak to valley height), R_q (the root-mean-square deviation of a profile), R_a (the average value of profile deviation from the mean line), and R_{sm} (average peak spacing) (Mitutoyo Corporation, 2014; EN ISO 4287, 1998). The numerical values of these parameters for the studied alloy surfaces are given in the inserted tables in Fig. 5. After mechanical abrasion, a relatively smooth surface was obtained (Fig. 5(a)). The values of all the roughness profile parameters are less than unity. The surface texture was seriously disrupted upon exposure of the sample to 3.5 wt.% NaCl solution. The surface in Fig. 5(b) appears very rough and well-differentiated peaks and valleys can be clearly seen. It is justifiable to assert that, the alloy sample corroded severely in the NaCl solution. As could be seen in the inserted table in Fig. 5(b), the roughness characteristics of the surface are almost seven times that of the abraded sample (Fig. 5(a)). For instance, 0.070 µm was measured as the average peak to valley height (R_z) on the surface in Fig. 5(b) whereas the value stood at 0.308 µm in the abraded surface. The values of other parameters measured on the corroded surface are three-seven times those of the abraded surface.

There was a significant reduction in the roughness characteristics of the sample surface when it was exposed to the corrosive solution containing the natural polymers. Clearly, it is seen that the surfaces in Fig. 5(c) & (d) are smoother compared to the one in Fig. 5(b). By comparing the values of the roughness parameters in the inserted tables in Fig. 5(c) & (d) to those in Fig. 5(b), the values of the roughness parameters of the inhibited surfaces are remarkably smaller. In fact, the R_z, R_c, and R_t parameters are almost 80 % smaller than those in Fig. 5(b). This corroborates the experimental results that HEC and ALG inhibited the corrosion of AZ31 Mg alloy in 3.5 wt.% NaCl solution.

The outstanding inhibition performance of the HEC- and ALG-formulations towards the alloy degradation in the studied medium is also obvious in the AFM studies. The surfaces of the 2-D and 3-D images in Fig. 5(e) and (f) is comparable to the one in Fig. 5(a). It is interesting to note that, just like the abraded surface (Fig. 5(a)), all the values of the roughness parameters in Fig. 5(e) and (f) are less than unity. This clearly shows the effectiveness of the formulations in retarding the dissolution of the alloy in the NaCl solution. This may have been possible through the adsorption of substantial amount of the formulations components on the sample surfaces, which effectively obstructed the penetration of corrosive agents to the surfaces. A comparison of Fig. 5(e) and (f) reveals that the HEC-formulations (Fig. 5(e)) was slightly better than the ALG-formulations, which is in agreement with other experimental results (Tables 2 and 3, Fig. 4).

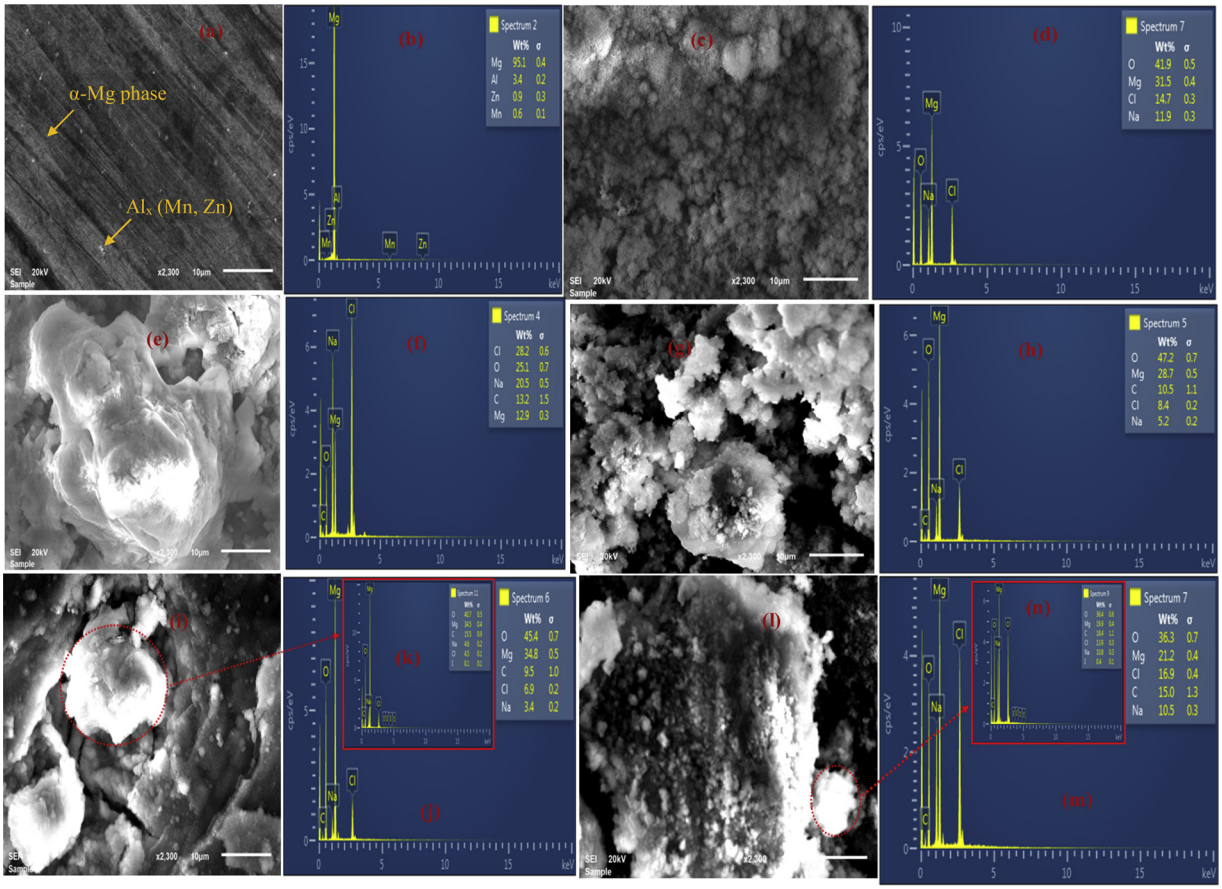

Fig. 6. SEM images and EDX spectra for AZ31 Mg alloy after (a, b) mechanical abrasion and immersion in 3.5 wt.% NaCl solution (c, d) without and with (e, f) HEC, (g, h) ALG, (i k) HEC-formulation, (l, m, n) ALG-formulation for 24 h under normal atmospheric condition.

3.2.3. SEM and EDX studies

Fig. 6 presents the SEM pictures and EDX spectra for AZ31 Mg alloy (a, b) after mechanical abrasion and after immersion in 3.5 wt.% NaCl solution (c, d) without and with (e, f) HEC, (g, h) ALG, (i, j, k) HEC-formulation, (l, m, n) ALG-formulation for 24 h at 25 °C. After abrasion, the surface was relatively smooth (Fig. 6(a)) and the α-Mg phase and the alloying elements phase can easily be distinguished. The corresponding EDX spectrum (Fig. 6(b)) shows the weight composition of Mg on the surface to be 95.1 % and that of Al as 3.4 %. By immersing the sample in 3.5 wt.% NaCl solution for 24 h, the surface morphology becomes rougher (Fig. 6(c)) and the weight percentage of Mg on the surface reduced to 31.5 %. The alloying elements (Al, Zn, & Mn) were undetected. These points to serious corrosion of the alloy in the studied medium. Additionally, salt-like corrosion products are seen on the surface in Fig. 6(c). The EDX spectrum in Fig. 6(d) reveals that, Na (11.9 %), O (41.9 %), and Cl (14.7 %) are the elemental composition of the corrosion products. It has been widely reported (Esmaily et al., 2017; Song, 2005) that $Mg(OH)_2$ precipitate is the main corrosion product during the corrosion of Mg in neutral and alkaline media. Nevertheless, $Mg(OH)_2$ precipitate exhibits slight inhibiting effect (Song, 2006). Because the $Mg(OH)_2$ layer is porous (Fig. 6(c)), the slight protection effect cannot be sustained as aggressive ions would still penetrate the layer, attack the surface, and induce corrosion. On the alloy surfaces exposed to NaCl solution containing the natural polymers or their formulations (Fig. 6(e, g, i, & l)), it is seen that a more compact and dense product layers were formed. These films may have effectively prevented the ingression of corrosive ions into the alloy surface and by so doing protected the metal against corrosion. The EDX spectra in Fig. 6(f, h, j, & m) clearly show that the products on the surfaces in Fig. 6(e, g, i, & l) were of different composition from the one on the surface of Fig. 6(c). The presence of C in substantial amount in Fig. 6(f, h, j, & m) and it absent in Fig. 6(d) confirms the adsorption of organic matter on the surfaces in Fig. 6(e, g, i, & l). When the entire surfaces of Fig. 6 (i & l) were scanned, the element, I was not detected but was found when the scan was concentrated on a deposited product (Fig. 6 (k & n)). This shows the insensitivity of the EDX instrument.

3.2.4. FTIR and UV–vis studies

FTIR experiments were undertaken for pure HEC and ALG as well as the adsorbed products extracted from the surfaces of the samples immersed in 3.5 wt.% NaCl solution containing the polymers for 24 h. The comparative spectra are shown in Fig. S3. In Fig. S(a), prominent peaks are seen at 1052 cm^{-1}, 1353 cm^{-1}, 2874 cm^{-1}, and 3372 cm^{-1} in the pure HEC spectrum. The strong and sharp peak at 1052 cm^{-1} is allotted to the stretching vibration of ether C—O (Sun, Wang, & Yan, 2017) while the weak peak at 1353 cm^{-1} is assigned to O—H bending vibration (Orhan, Ziba, Morcali, & Dolaz, 2018). The peaks at 2874 cm^{-1} and 3372 cm^{-1} are linked to the C—H and O—H stretching vibrations (Orhan et al., 2018), respectively. Compared with the FTIR spectrum of HEC-film (Fig. S3(a)), the ether C—O and the C—H stretching peaks almost completely disappeared while an extra peak appeared at 3691 cm^{-1}. The additional peak is assigned to the stretching vibration of O—H in $Mg(OH)_2$ (Pilarska, Wysokowski, Markiewicz, & Jesionowski, 2013).The disappearance of the peaks suggest the involvement of the ether functional groups in HEC in the adsorption process. Similar submission can be found in the literature (Haladu, Umoren, Ali, Solomon, & Mohammed, 2019).

Fig. S3(b) shows the comparative spectra for pure ALG and ALG-film. The characteristic peaks in the pure ALG spectrum are the pyranosyl ring C—O stretching peak at 1026 cm^{-1} (Daemi & Barikani,

2012), the symmetric and asymmetric vibrational peaks of the carboxylate salt at 1406 cm^{-1} and 1595 cm^{-1} (Daemi & Barikani, 2012), respectively, and the O—H stretching band at 3233 cm^{-1}. The ALG-film spectrum, although very similar to that of the pure ALG differ from the later in the appearance of the O—H ($Mg(OH)_2$) stretching peak at 3691 cm^{-1} and the remarkable reduction in the intensity of the pyranosyl ring C—O stretching and the symmetric and asymmetric vibrational peaks of the carboxylate salt. This suggests the participation of —COONa group in the adsorption of ALG molecules onto the alloy surface. The appearance of the O–H ($Mg(OH)_2$) vibrational peak at 3693 cm^{-1} and 3691 cm^{-1}, respectively in the ALG-film and HEC-film spectra is suggestive of $Mg(OH)_2$ as the corrosion product on the alloy surface.

Fig. S3(c) presents the UV–vis spectra obtained for a solution of 3.5 wt.% NaCl without and with the studied polymers (HEC or ALG) after immersing a AZ31 Mg sample for 24 h. In the blank solution spectrum, a sharp absorption peak is observed at 205 nm and is consistent with hydroxide (Zuman & Szafranski, 1976). This confirms the existence of $Mg(OH)_2$ in the corrosion product as earlier suggested by the FTIR results (Fig. S3(a & b)). In the spectrum of the polymer containing solution, a weak peak at 343 nm is observed in addition to the sharp hydroxide peak at 205 nm. The appearance of the new peak at 343 nm justify the formation of Mg-polymer complex. Similar submission can be found in the corrosion literature (Abdel-Rehim, Khaled, & Abd-Elshafi, 2006; Haladu et al., 2019).

3.3. Mechanism of inhibition by HEC- and ALG-formulations

To gain insight into the corrosion and corrosion inhibition mechanism of AZ31 Mg alloy by HEC- and ALG-formulations, the products deposited on the specimen surfaces after immersing in 3.5 wt.% NaCl solution without and with the formulation for 24 h were analyzed using the XPS technique. Fig. 7 presents the high-resolution spectra of Mg 1s, Cl 2p, C 1s, O 1s, and I 3d obtained from the analysis of the XPS results.

In the Mg 1s spectrum in Fig. 7(i), (v) and (x), a single peak at 1304.91 eV, 1304.96 eV, and 1304.98 eV, respectively is observed and corresponds to $Mg(OH)_2$ (Li, Liu, Lei, & Xiao, 2015; Nabizadeh et al., 2019). This is in agreement with the FTIR and UV–vis results (Section 3.2.4) and confirms that, $Mg(OH)_2$ is the main corrosion product on the alloy surface. The peak at 197.58 eV (Fig. 7(ii)), 197.99 eV (Fig. 7(vi)), and 197.63 (Fig. 7(xi)) in the O 1s high-resolution spectra is consistent with the OH^- group (Kumar, Hassan, Sorour, Paramsothy, & Gupta, 2018). The electrochemical cathodic reduction of water produces OH-ions (Dindodi & Shetty, 2014):

$$2H_2O + 2e- \rightarrow H_2\,(g) + 2OH- \quad (13)$$

It was reported (Cai, Lu, Li, Liang, & Zhou, 2009; Lopez & Natta, 2001) that at active potential of about -1.56 V vs. Ref. (the range of potential of the present work), magnesium is simultaneously oxidized to Mg^+ and Mg^{2+} ions:

$$Mg \rightarrow Mg^+ + e^- \quad (14)$$

$$Mg \rightarrow Mg^{2+} + 2e^- \quad (15)$$

The Mg^+ ion is unstable and readily oxidize to Mg^{2+} (Dindodi & Shetty, 2014). The Mg^{2+} ions so-generated react with the OH^- ions from the cathodic region to form the main corrosion product, $Mg(OH)_2$ (Eq. (16)).

$$2Mg^+ + 2OH^- \rightarrow Mg(OH)_2 \quad (16)$$

Beside the $Mg(OH)_2$ as the main corrosion product, Cl-containing compounds such $MgCl_2$ and $Mg_2(OH)_3Cl$ (Cui et al., 2018) co-existed on the surface. The Cl $2p_{3/2}$ peak originated from the Cl-containing compounds can be clearly seen at 197.58 eV, 197.99 eV, and 197.63 eV in Fig. 7(iii), (vii) & (xii), respectively

It is obvious that the inhibitor molecules were adsorbed on the alloy surface and by extension protected the surface against corrosion. In the C 1s spectrum of the blank (Fig. 7(iv)), a single peak at 285.11 eV is

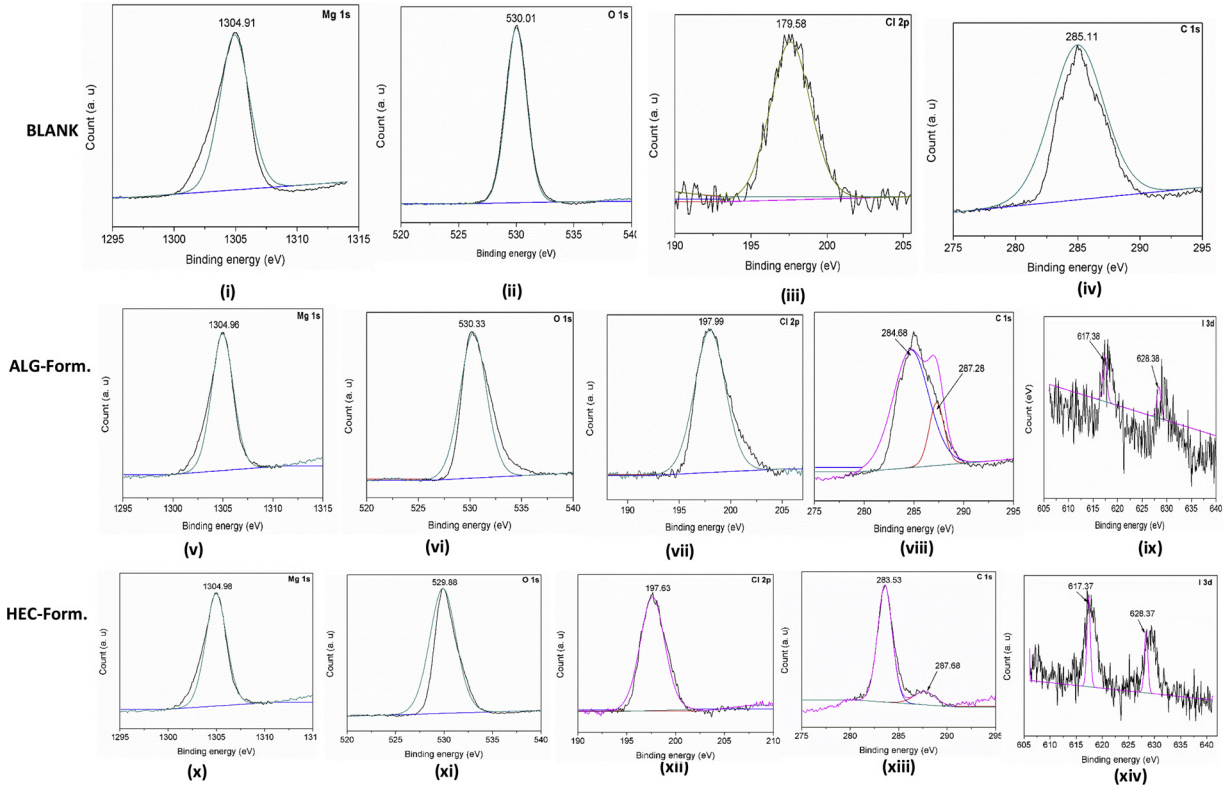

Fig. 7. High-resolution spectra of film formed on AZ31 Mg alloy immersed in 3.5 wt.% NaCl solution (i-iv) without and with (v-ix) ALG-formulation, (x-xiv) HEC-formulation for 24 h under normal atmospheric condition.

seen and is associated with the contaminative C−C/C-H groups (Cui et al., 2018). Compared with the C 1s spectra in Fig. 7(viii) and (xiii), an additional peak at 287.28 eV and 287.68 eV, respectively is seen and belong to $-COO^{-}/-CO^{-}$ groups (Umoren et al., 2019; Zhang, He, & Gu, 2006) of the inhibitor. It was reported that Date palm oil contained oleic acid ($C_{18}H_{34}O_2$), lauric acid ($C_{12}H_{24}O_2$), stearic acid ($C_{18}H_{36}O_2$), palmitic acid ($C_{16}H_{32}O_2$), and linolenic acid ($C_{18}H_{30}O_2$) (Nehdi, Sbihi, Tan, Rashid, & Al-Resayes, 2018) as the main chemical components. It therefore infers that the $-COO^{-}/-CO^{-}$ groups from the inhibitor components interacted with the metal surface to form the protective layer, which is in excellent agreement with the FTIR results (Section 3.2.4) and the report of Hou et al. (2016). Additionally, iodide ions, a component of the formulation was detected on the surfaces of the inhibited samples. In the I 3d spectrum in Fig. 7(ix), two peaks typical of I $3d_{3/2}$ and I $3d_{5/2}$ are observed at 617. 38 eV and 628.38 eV, respectively. Similar peaks are seen at 617.37 eV and 628.37 eV in the I 3d spectrum in Fig. 7(xiv). The peak at approximately 617 eV is assigned to triiodide (I_3^-) (Kalita, Wakita, Takahashi, & Umeno, 2011; Solomon et al., 2018) while the band at approximately 628 eV is consistent with pentaiodide (I_5^-) (Kalita et al., 2011; Solomon et al., 2018).

From the above results, a co-adsorption inhibition mechanism is proposed. The surface of AZ31 Mg alloy immersed in 3.5 wt.% NaCl solution is covered with porous $Mg(OH)_2$ film. The natural polymers (HEC and ALG), through hydroxyl and/or carboxyl functional group chelated with the alloy surface (Hou et al., 2016). The Mg-polymer complex did not significantly changed the characteristic porosity of the surface film, as indicated by the low inhibition efficiency values (Tables 2 and 3). In the presence of the Date palm oil and the potassium iodide, Mg^{2+} and other cations on the surface act as a bridge (Zhang, Li, Li, Zhang, & Wang, 2015), so that the carboxylate ions from the oil and iodide ions co-adsorb on the surface. The co-adsorption of the multicomponent gives rise to a compact protective film on the alloy surface as evidenced in the SEM images (Fig. 6(i & l)).

4. Summary and conclusion

Seven natural polymers (CMC, PEC, GA, CHI, HEC, ALG, and Dex) were screened as corrosion inhibitor for AZ31 Mg alloy in 3.5 wt.% NaCl solution. CMC, PEC, GA, CHI, and Dex accelerated corrosion while HEC and ALG moderately inhibited corrosion. The corrosion acceleration effect was linked to chelates formation between the natural polymers and Mg^{2+} ions in the electrolyte rather than on the alloy surface (Lamaka et al., 2017). In the case of HEC and ALG, the complex was formed on the substrate surface and retarded both the anodic Mg dissolution reaction and the cathodic gas evolution reaction. Studies on the effect of concentration of HEC and ALG on inhibition efficiency reveal that, protection performance was maximum when one gram of inhibitor per liter of solution was used. With this concentration, up to 64.13 % and 58.27 % inhibition efficiency is achievable for HEC and ALG, respectively. In an attempt to effectively protect the alloy against corrosion, two inhibitor formulations consisting of either HEC or ALG, potassium iodide, and Date palm seeds oil were formulated. The formulations were found to effectively protect the alloy surface against corrosion in 3.5 wt.% NaCl solution yielding up to 80 % inhibition efficiency. Surface observation studies using SECM, AFM, SEM and EDX conform to other experimental results; they clearly show the better corrosion protection afforded by the inhibitor formulations than the polymers alone. Results from all the applied techniques reveal that HEC and HEC-formulations were better inhibitor than ALG and ALG-formulations. FTIR, UV–vis, and XPS results reveal that $Mg(OH)_2$ is the main corrosion product that co-existed with adsorbed inhibitor complexes on the alloy surface, which is in agreement with previous studies (Dindodi & Shetty, 2014; Lopez & Natta, 2001; Saji, 2019). We conclude that, HEC and ALG are promising cheap and green sources for the formulation of corrosion inhibitor for Mg and its alloys. The application of Mg and its alloy is at present limited because of lack of effective corrosion inhibitors.

Acknowledgements

The authors acknowledge funding from the Research and Development (R&D) Program (Research Pooling Initiative), Ministry of Education, Riyadh, Saudi Arabia.

Appendix A. Supplementary data

Supplementary material related to this article can be found, in the online version, at doi:https://doi.org/10.1016/j.carbpol.2019.115466.

References

Abdel-Rehim, S. S., Khaled, K. F., & Abd-Elshafi, N. S. (2006). Electrochemical frequency modulation as a new technique for monitoring corrosion inhibition of iron in acid media by new thiourea derivative. *Electrochimica Acta, 51*, 3269–3277.

ASTM-G1–03 (2017). *Standard practice for preparing, cleaning, and evaluation corrosion test specimens.* ASTM Book of Standards (Reapproved 2017).

Bayol, E., Gürten, A. A., Dursun, M., & Kayakirilmaz, K. (2008). Adsorption behavior and inhibition corrosion effect of sodium carboxymethyl cellulose on mild steel in acidic medium. *Acta Physico-Chimica Sinica, 24*, 2236–2243.

Bello, M., Ochoa, N., Balsamo, V., López-Carrasquero, F., Coll, S., Monsalve, A., et al. (2010). Modified cassava starches as corrosion inhibitors of carbon steel: An electrochemical and morphological approach. *Carbohydrate Polymers, 82*, 561–568.

Bentrah, H., Rahali, Y., & Chala, A. (2014). Gum Arabic as an eco-friendly inhibitor for API 5L X42 pipeline steel in HCl medium. *Corrosion Science, 82*, 426–431.

Biswas, A., Pal, S., & Udayabhanu, G. (2015). Experimental and theoretical studies of xanthan gum and its graft co-polymer as corrosion inhibitor for mild steel in 15% HCl. *Applied Surface Science, 353*, 173–183.

Cai, Z., Lu, D., Li, W., Liang, Y., & Zhou, H. (2009). Study on anodic oxidation of magnesium in 6M KOH solution by alternative current impedance. *International Journal of Hydrogen Energy, 34*, 467–472.

Cao, F. Y., Shi, Z. M., Hofstetter, J., Uggowitzer, P. J., Song, G. L., Liu, M., et al. (2013). Corrosion of ultra-high-purity Mg in 3.5% NaCl solution saturated with $Mg(OH)_2$. *Corrosion Science, 75*, 78–99.

Chen, X. B., Birbilis, N., & Abbott, T. B. (2011). Review of corrosion-resistant conversion coatings for magnesium and its alloys. *Corrosion, 67*, 1–16. https://doi.org/10.5006/1.3563639.

Chirkunov, A. A., & Zheludkevich, M. L. (2018). Corrosion inhibition of Elektron WE43 magnesium alloy in NaCl solution. *International Journal of Corrosion and Scale Inhibition, 7*, 376–389.

Crini, G., Morin-Crini, N., Fatin-Rouge, N., De´on, S., & Fievet, P. (2017). Metal removal from aqueous media by polymer-assisted ultrafiltration with chitosan. *Arabian Journal of Chemistry, 10*, S3826–S3839.

Cui, Z., Ge, F., Lin, Y., Wang, L., Lei, L., Tian, H., et al. (2018). Corrosion behavior of AZ31 magnesium alloy in the chloride solution containing ammonium nitrate. *Electrochimica Acta, 278*, 421–437.

Daemi, H., & Barikani, M. (2012). Synthesis and characterization of calcium alginate nanoparticles, sodium homopolymannuronate salt and its calcium nanoparticles. *Scientia Iranica F, 19*(6), 2023–2028.

Dindodi, N., & Shetty, A. N. (2014). *Stearate as a green corrosion inhibitor of magnesium alloy ZE41 in sulfate medium.* https://doi.org/10.1016/j.arabjc.2014.11.028.

El-Haddad, M. N. (2013). Chitosan as a green inhibitor for copper corrosion in acidic medium. *International Journal of Biological Macromolecules, 55*, 142–149.

EN ISO 4287 (1998). *Geometrical Product Specifications (GPS) − Surface texture: Profile methods − terms, definitions, and surface parameters*.

Esmaily, M., Svensson, J. E., Fajardo, S., Birbilis, N., Frankel, G. S., Virtanen, S., et al. (2017). Fundamentals and advances in magnesium alloy corrosion. *Progress in Materials Science, 89*, 92–193.

Fares, M. M., Maayta, A. K., & Al-Qudah, M. M. (2012). Pectin as promising green corrosion inhibitor of aluminum in hydrochloric acid solution. *Corrosion Science, 60*, 112–117.

Fares, M. M., Maayta, A. K., & Al-Mustafa, J. A. (2012). Corrosion inhibition of iota-carrageenan natural polymer on aluminum in presence of zwitterion mediator in HCl media. *Corrosion Science, 65*, 223–230.

Finšgar, M., & Jackson, J. (2014). Application of corrosion inhibitors for steels in acidic media for the oil and gas industry: A review. *Corrosion Science, 86*, 17–41.

Frignani, A., Grassi, V., Zanotto, F., & Zucchi, F. (2012). Inhibition of AZ31 Mg alloy corrosion by anionic surfactants. *Corrosion Science, 63*, 29–39.

Gray, J. E., & Luan, B. (2002). Protective coatings on magnesium and its alloys-a critical review. *Journal of Alloys and Compounds, 336*, 88–113.

Haladu, S. A., Umoren, S. A., Ali, S. A., Solomon, M. M., & Mohammed, A. I. (2019). Synthesis, characterization and electrochemical evaluation of anticorrosion property of a tetrapolymer for carbon steel in strong acid media. *Chinese Journal of Chemical Engineering, 27*, 965–978.

Hou, L., Dang, N., Yang, H., Liu, B., Li, Y., Wei, Y., et al. (2016). The electrochemical society a combined inhibiting effect of sodium alginate and sodium phosphate on the corrosion of magnesium alloy AZ31 in NaCl solution. *Journal of the Electrochemical Society, 163*(8), C486–C494.

Jamali, S. S., Moulton, S. E., Tallman, D. E., Forsyth, M., Weber, J., & Wallace, G. G. (2014). Applications of scanning electrochemical microscopy (SECM) for local characterization of AZ31 surface during corrosion in a buffered media. *Corrosion Science, 86*, 93–100.

Jamali, S. S., Moulton, S. E., Tallman, D. E., Forsyth, M., Weber, J., Mirabedini, A., et al. (2015). Corrosion protection afforded by praseodymium conversion film on Mg alloy AZNd in simulated biological fluid studied by scanning electrochemical microscopy. *Journal of Electroanalytical Chemistry, 739*, 211–217.

Jamali, S. S., Moulton, S. E., Tallman, D. E., Forsyth, M., Weber, J., & Wallace, G. G. (2015). Evaluating the corrosion behaviour of Magnesium alloy in simulated biological fluid by using SECM to detect hydrogen evolution. *Electrochimica Acta, 152*, 294–301.

Kalita, G., Wakita, K., Takahashi, M., & Umeno, M. (2011). Iodine doping in solid precursor-based CVD growth graphene film. *Journal of Material Chemistry, 21*, 15209–15213.

King, A. D., Birbilis, N., & Scully, J. R. (2014). Accurate electrochemical measurement of magnesium corrosion rates; a combined impedance, mass-loss and hydrogen collection. *Electrochimica Acta, 121*, 394–406.

Kumar, A. M., Kwon, S. H., Jung, H. C., Park, Y. H., Kim, H. J., & Shin, K. S. (2014). Fabrication and electrochemical corrosion behavior of PEO coatings on strip-cast AZ31 Mg alloy in 3.5% NaCl solution. *Industrial & Engineering Chemistry Research, 53*, 9703–9713.

Kumar, A. M., Hassan, S. F., Sorour, A. A., Paramsothy, M., & Gupta, M. (2018). Electrochemical corrosion and in vitro biocompatibility performance of AZ31Mg/Al2O3 nanocomposite in simulated body fluid. *Journal of Materials Engineering and Performance, 27*, 3419–3428.

Kumar, A. M., Hassan, S. F., Sorour, A. A., Paramsothy, M., & Gupta, M. (2019). Investigation on the controlled degradation and invitro mineralization of carbon nanotube reinforced AZ31 nanocomposite in simulated body fluid. *Metals and Materials International, 25*, 105–116.

Lamaka, S. V., Vaghefinazari, B., Mei, D., Petrauskas, R. P., Höche, D., & Zheludkevich, M. L. (2017). Comprehensive screening of Mg corrosion inhibitors. *Corrosion Science, 128*, 224–240.

Li, K., Liu, J., Lei, T., & Xiao, T. (2015). Optimization of process factors for self-healing vanadium-based conversion coating on AZ31 magnesium alloy. *Applied Surface Science, 353*, 811–819.

Lopez, M. G., & Natta, B. (2001). Evidence of two anodic processes in the polarization curves of magnesium in aqueous media. *Corrosion, 712*, 5006–5015.

Lu, X., Li, Y., Ju, P., Chen, Y., Yang, J., Qian, K., et al. (2019). Unveiling the inhibition mechanism of an effective inhibitor for AZ91 Mg alloy. *Corrosion Science, 148*, 264–271.

Mei, D., Lamaka, S. V., Feiler, C., & Zheludkevich, M. L. (2019). The effect of small-molecule bio-relevant organic components at low concentration on the corrosion of commercially pure Mg and Mg-0.8Ca alloy: An overall perspective. *Corrosion Science, 153*, 258–271.

Mena-Morcillo, E., Veleva, L., & Wipf, D. O. (2018). In situ investigation of the initial stages of AZ91D magnesium alloy biodegradation in simulated body fluid. *International Journal of Electrochemical Science, 13*, 5141–5150.

Mitutoyo Corporation (2014). *Surface finish analysis.* 1–58 (https://www.mitutoyo.com/wp-content/uploads/2012/···/1984_Surf_Roughness_PG.pd).

Mobin, M., & Rizvi, M. (2016). Inhibitory effect of xanthan gum and synergistic surfactant additives for mild steel corrosion in 1 M HCl. *Carbohydrate Polymers, 136*, 384–393.

Nabizadeh, M., Sarabi, A. A., & Eivaz Mohammadloo, H. (2019). Comparative investigation of Cu ion and adipic acid addition on electrochemical and microstructure characteristics of vanadium conversion coating on AZ31 Mg alloy. *Surface & Coatings Technology, 357*, 1–11.

Nehdi, I. A., Sbihi, H. M., Tan, C. P., Rashid, U., & Al-Resayes, S. I. (2018). Chemical composition of Date palm (*Phoenix dactylifera L.*) seed oil from six Saudi Arabian cultivars. *Journal of Food Science, 83*, 624–630.

NACE Standard Test Method TM0193 (2016). *Laboratory corrosion testing of metals in static chemical cleaning solutions at temperatures below 93 °C (200 °F)* (Reaffirmed 2016 – 04–05).

Orhan, B., Ziba, C. A., Morcali, M. H., & Dolaz, M. (2018). Synthesis of hydroxyethyl cellulose from industrial waste using microwave irradiation. *Sustainable Environment Research, 28*, 403–411.

Pavithra, M. K., Venkatesha, T. V., Vathsals, K., & Nayana, K. O. (2010). Synergistic effect of halide ions on improving corrosion inhibition behaviour of benzisothiozole-3-piperizine hydrochloride on mild steel in 0.5M H_2SO_4 medium. *Corrosion Science, 52*, 3811–3819.

Pilarska, A., Wysokowski, M., Markiewicz, E., & Jesionowski, T. (2013). Synthesis of magnesium hydroxide and its calcinates by a precipitation method with the use of magnesium sulfate and poly(ethylene glycols). *Powder Technology, 235*, 148–157.

Qiao, Z. X., Shi, Z. M., Hort, N., Abidin, N. I. Z., & Atrens, A. (2012). Corrosion behaviour of a nominally high purity Mg ingot produced by permanent mould direct chill casting. *Corrosion Science, 61*, 185–207.

Rajeswari, V., Kesavan, D., Gopiraman, M., & Viswanathamurth, I. P. (2013). Physicochemical studies of glucose, gellan gum, and hydroxypropyl cellulose - Inhibition of cast iron corrosion. *Carbohydrate Polymers, 95*, 288–294.

Salleh, S. H., Thomas, S., Yuwono, J. A., Venkatesan, K., & Birbilis, N. (2015). Enhanced hydrogen evolution on Mg $(OH)_2$ covered Mg surfaces. *Electrochimica Acta, 161*, 144–152.

Saji, V. S. (2019). Organic conversion coatings for magnesium and its alloys. *Journal of Industrial and Engineering Chemistry, 75*, 20–37.

Singl, W. P., & Bockris, J. O. (1996). *Toxicity issues of organic corrosion inhibitors: Application of QSAR model. Corrosion*. TX: Houston Paper No. 225.

Sviatlana, L., Daniel, D., Carsten, B., & Mikhail, Z. (2017). *Corrosion inhibitor composition for magnesium or magnesium alloys.* WO 2017/064185.

Solmaz, R., Kardas, G., ulha, M. C., Yazıcı, B., & Erbil, M. (2008). Investigation of adsorption and inhibitive effect of 2-mercaptothiazoline on corrosion of mild steel in hydrochloric acid media. *Electrochimica Acta, 53*, 5941–5952.

Solomon, M. M., Gerengi, H., & Umoren, S. A. (2017). Carboxymethyl cellulose/silver nanoparticles composite: Synthesis, characterization and application as a benign corrosion inhibitor for St37 steel in 15% H_2SO_4 medium. *ACS Applied Materials & Interfaces, 9*, 6376–6389.

Solomon, M. M., Umoren, S. A., Obot, I. B., Sorour, A. A., & Gerengi, H. (2018). Exploration of dextran for application as corrosion inhibitor for steel in strong acid environment: Effect of molecular weight, modification, and temperature on efficiency. *ACS Applied Materials & Interfaces, 10*, 28112–28129.

Song, G. (2005). Recent progress in corrosion and protection of magnesium alloys. *Advanced Engineering Materials, 7*, 563–586.

Song, G. (2006). *The corrosion and protection of magnesium alloys.* Beijing: Chemical Industry Press of China ISBN 7-5025-8565-6.

Sun, N., Wang, T., & Yan, X. (2017). Synthesis and investigation of a self-assembled hydrogel based on hydroxyethyl cellulose and its in vitro ibuprofen drug release characteristics. *RSC Advances, 7*, 9500–9511.

Umoren, S. A., Ogbobe, O., Igwe, I. O., & Ebenso, E. E. (2008). Inhibition of mild steel corrosion in acidic medium using synthetic and naturally occurring polymers and synergistic halide additives. *Corrosion Science, 50*, 1998–2006.

Umoren, S. A., Solomon, M. M., Udosoro, I. I., & Udoh, A. P. (2010b). Inhibitive and adsorption behaviour of carboxymethyl cellulose on mild steel corrosion in sulphuric acid solution. *Corrosion Science, 52*, 1317–1325.

Umoren, S. A., Solomon, M. M., Udosoro, I. I., & Udoh, A. P. (2010a). Synergistic and antagonistic effects between halide ions and carboxymethyl cellulose for the corrosion inhibition of mild steel in sulphuric acid solution. *Cellulose, 17*, 635–648.

Umoren, S. A., Banera, M. J., Alonso-Garcia, T., Gervasi, C. A., & Mirifico, M. V. (2013). Inhibition of mild steel corrosion in HCl solution using chitosan. *Cellulose, 20*, 2529–2545.

Umoren, S. A., Obot, I. B., Madhankumar, A., & Gasem, Z. M. (2015). Performance evaluation of pectin as ecofriendly corrosion inhibitor for X60 pipeline steel in acid medium: Experimental and theoretical approaches. *Carbohydrate Polymers, 124*, 280–291.

Umoren, S. A., & Solomon, M. M. (2019). Protective polymeric films for industrial substrates: A critical review on past and recent applications with conducting polymers and polymer composites/nanocomposites. *Progress in Materials Science, 104*, 380–450.

Umoren, S. A., Solomon, M. M., Ali, S. A., & Dafalla, H. D. M. (2019). Synthesis, characterization, and utilization of a diallylmethylamine-based cyclopolymer for corrosion mitigation in simulated acidizing environment. *Materials Science and Engineering C, 100*, 897–914.

Zalloum, H. M., & Mubarak, M. S. (2013). Chitosan and chitosan derivatives as chelating agents. In S. Thomas, N. Ninan, S. Mohan, & E. Francis (Vol. Eds.), *Natural polymers, biopolymers, biomaterials, and their composites, blends, and IPNs, advances in materials science: volume 2*. Toronto: Apple Academic Press.

Zhang, L., He, R., & Gu, H. C. (2006). Oleic acid coating on the monodisperse magnetite nanoparticles. *Applied Surface Science, 253*, 2611–2617.

Zhang, J., & Wu, C. (2010). Corrosion and protection of magnesium alloys. *Recent Patents on Corrosion Science, 2*, 55–68.

Zhang, P., Li, Q., Li, L. Q., Zhang, X. X., & Wang, Z. W. (2015). A study of environment-friendly synergistic inhibitors for AZ91D magnesium alloy. *Materials and Corrosion, 66*, 31–34.

Zuman, P., & Szafranski, W. (1976). Ultraviolet spectra of hydroxide, alkoxide, and hydrogen sulfide anions. *Analytical Chemistry, 48*, 2162–2163.